Polycarbon Ligand Chemistry: Electronic Interactions between a Mononuclear Ruthenium Fragment and a Cobalt−Carbon Cluster Core

Paul J. Low,† Roger Rousseau,† Pikka Lam,† Konstantin A. Udachin,† Gary D. Enright,† John S. Tse,*,† Danial D. M. Wayner,† and Arthur J. Carty*,†,‡

Steacie Institute for Molecular Sciences, 100 Sussex Drive, Ottawa, Ontario, K1A 0R6, Canada, and Ottawa-Carleton Research Institute, Department of Chemistry, University of Ottawa, 1125 Colonel By Drive, Ottawa, Ontario, K1S 5B6, Canada

Received April 22, 1999

The preparation, characterization, and electrochemical response of the complexes $Co_2(\mu\text{-}Me_3SiC{\equiv}CC_2C{\equiv}CSiMe_3)(CO)_4(dppm)$ (**2**) and $Co_2(\mu\text{-}Me_3SiC_2C{\equiv}CC{\equiv}CSiMe_3)(CO)_4(dppm)$ (**3**) are described. Metalation of one of the pendant alkynyl groups in each complex has been achieved, yielding $Co_2\{\mu\text{-}Me_3SiC{\equiv}CC_2C{\equiv}C[Ru(PPh_3)_2Cp]\}(CO)_4(dppm)$ (**4**) and $Co_2\{\mu\text{-}Me_3SiC_2C{\equiv}CC{\equiv}C[Ru(PPh_3)_2Cp]\}(CO)_4(dppm)$ (**5**). The spectral and electrochemical properties of the heterometallic complexes indicate a significant electronic interaction between the mononuclear fragment and the metallocarbon cluster core. The electronic structure of these compounds has been modeled using DFT, ZINDO, and ELF calculations, and an explanation of the nature of the electronic interaction between the heterometallic fragments is presented.

Introduction

The construction of molecules in which redox-active subunits are linked by a bridging ligand capable of transmitting electronic effects has become an area of immense interest in recent years. It is thought that these compounds may find application in the construction of molecular scale electronic devices[1] or display useful bulk properties, including magnetism,[2] electron transfer,[3] and large nonlinear optical response.[4]

Acetylene-based bridging ligands have been extensively examined during the course of these studies as the acetylene group is compatible with a wide range of redox probes, such as substituted organic aromatic groups,[5] porphyrins,[6] metallocenes,[7] mononuclear transition metal centers,[8] and transition metal clusters.[9] Unbranched polyyndiyl ligands $-(C{\equiv}C)_n-$ appear to be especially efficient in promoting electronic interactions, as connection between the end-capping groups is largely unaffected by the relative orientation[10] or aromaticity[11] of a spacing group.

Electronic "communication" between organometallic fragments linked by pure polyynyl ligands, $-(C{\equiv}C)_n-$, has been described by Gladysz,[12] Lapinte,[13] and Bruce[14] for mononuclear systems and by Osella[15] and Robinson[16] for multimetallic systems. Several theoretical studies

* Corresponding author. E-mail: Arthur.Carty@nrc.ca. Fax: +1 613 957 8850.
† Steacie Institute for Molecular Sciences.
‡ Ottawa-Carleton Research Institute.

(1) (a) Ward, M. D. *Chem. Soc. Rev.* **1995**, 121. (b) Ward, M. *Chem. Ind.* **1997**, 640. (c) Grosshenny, V.; Harriman, A.; Hissler, M.; Ziessel, R. *Platinum Met. Rev.* **1996**, *40*, 26. (d) Petty, M. C.; Bryce, M. R.; Bloor, D. *Introduction to Molecular Electronics*; Oxford University Press: New York, 1995.

(2) (a) Posselt, D.; Badur, W.; Steiner M.; Baumgarten, M. *Synth. Met.* **1993**, *55*, 3299. (b) Hmyene, M.; Yassar, A.; Escorne, M.; Perchon-Guégan, A.; Garnier, F. *Adv. Mater.* **1994**, *6*, 564. (c) Cargill Thompson, A. M. W.; Gatteschi, D.; McCleverty, J. A.; Navas, J. A.; Rentschler, E.; Ward, M. D. *Inorg. Chem.* **1996**, *35*, 2701. (d) Ung, V. A.; Cargill Thompson, A. M. W.; Bardwell, D. A.; Gatteschi, D.; Jeffery, J. C.; McCleverty, J. A.; Totti, F.; Ward, M. D. *Inorg. Chem.* **1997**, *36*, 3447.

(3) (a) Carter, F. L. In *Electronic Devices II*; Marcel Dekker: New York, 1987. (b) Goppel, W., Zeigler, C., Eds. *Nanostructures Based on Molecular Materials*; VCH: Weinheim, 1992. (c) Lehn, J. M. *Supramolecular Chemistry*; VCH: Weinheim, 1995. (d) Tour, J. M. *Chem. Rev.* **1996**, *96*, 537.

(4) (a) Long, N. J. *Angew. Chem., Int. Ed. Engl.* **1995**, *34*, 21. (b) Kanis, D. R.; Ratner, M. A.; Marks, T. J. *Chem. Rev.* **1994**, *94*, 195. (c) Whittal, I. R.; McDonagh, A. M.; Humphrey, M. G.; Samoc, M. *Adv. Organomet. Chem.* **1998**, *42*, 291.

(5) (a) Brandsma, L. *Preparative Acetylenic Chemistry*, 2nd ed.; Elsevier Science Publishers: New York, 1988. (b) March, J. *Advanced Organic Chemistry*, 3rd ed.; Plenum: New York, 1985.

(6) (a) Anderson, H. L. *Inorg. Chem.* **1994**, *33*, 972. (b) Arnold, D. P.; Nitschinsk, L. *Tetrahedron* **1992**, *48*, 8781. (c) Arnold, D. P.; Heath, G. A.; James, D. A. *New J. Chem.* **1998**, *12*, 1377. (d) Anderson, H. L. *Tetrahedron Lett.* **1992**, *33*, 1101.

(7) (a) Rosenblum, M.; Brawn, N.; Papenmeier, J.; Applebaum, M. *J. Organomet. Chem.* **1966**, *6*, 173. (b) Hsung, R. P.; Chidsey, C. E. D.; Sita, L. R. *Organometallics* **1995**, *14*, 4808.

(8) (a) Nast, R. *Coord. Chem. Rev.* **1982**, *47*, 89. (b) Manna, J.; John, K. D.; Hopkins, M. D. *Adv. Organomet. Chem.* **1995**, *38*, 79.

(9) (a) Sappa, E.; Tiripicchio, A.; Braunstein, P. *Chem. Rev.* **1983**, *83*, 203. (b) Sappa, E.; Tiripicchio, A.; Braunstein, P. *Coord. Chem. Rev.* **1985**, *65*, 219. (c) Bruce, M. I. *J. Organomet. Chem.* **1985**, *257*, 417.

(10) Woitellier, S.; Launay, J. P.; Joachim, C. *Chem. Phys.* **1989**, *131*, 481.

(11) Taylor, P. N.; Wylie, A. P.; Huuskonen, J.; Anderson, H. L. *Angew. Chem., Int. Ed. Engl.* **1998**, *37*, 986.

(12) (a) Brady, M.; Weng, W.; Zhou, Y.; Seyler, J. W.; Amoroso, A. J.; Arif, A. M.; Böhme, M.; Frenking, G.; Gladysz, J. A. *J. Am. Chem. Soc.* **1997**, *119*, 775. (b) Bartik, T.; Bartik, B.; Brady, M.; Dembinski, R.; Gladysz, J. A. *Angew. Chem., Int. Ed. Engl.* **1996**, *35*, 414. (c) Brady, M.; Weng, W.; Gladysz, J. A. *J. Chem. Soc., Chem. Commun.* **1994**, 2655.

(13) (a) Le Narvor, N.; Toupet, L.; Lapinte, C. *J. Am. Chem. Soc.* **1995**, *117*, 7129. (b) Coat, F.; Lapinte, C. *Organometallics* **1996**, *15*, 477.

(14) Bruce, M. I.; Denisovich, L. I.; Low, P. J.; Peregudova, S. M.; Ustynyuk, N. A. *Mendeleev Commun.* **1996**, 200.

10.1021/om990290w CCC: $18.00
Publication on Web 09/13/1999

that address the issues relating to the extent of electronic interaction between metal-containing groups in related model compounds have also been undertaken.[17]

It has been suggested that transition metal clusters should function well as electron reservoirs, capable of both accepting and releasing electrons,[18] and as such these species may find some use in the construction of nanoscale electronic circuits.[19] In addition, the redox properties of mixed transition metal−main group cluster cores have also attracted a great deal of attention in their own right, as these compounds play a crucial role in biological electron transport cycles.[20] Therefore compounds in which multinuclear cluster cores are linked by polyynyl ligands would appear to have great potential for use in the construction of large electroactive molecular assemblies.

These observations have prompted something of a renaissance in the organometallic chemistry of polyynes. In addition to the studies mentioned above, many other groups have also been active in the preparation of compounds of the general type $[L_nM](C{\equiv}C)_x[ML_n]$.[21] Examples of compounds in which a polycarbon chain is capped at each end by a multinuclear cluster fragment include the following: tricobalt clusters linked by μ_3-η^1-carbon chains[22] and related $[MCo_2(CO)_8Cp]$ (M = Mo, W) species;[17c] a complex with an [MnMo(μ_2-η^1,η^1-C_2)-MnMo] core;[23] a series of compounds with $M_2(\mu\text{-}PPh_2)(CO)_6$ units (M = Fe, Ru) linked by μ_4-η^1,η^2-C_2 and μ_4-η^1,η^2:η^1,η^2-C_4 ligands;[24] the hexametallic complexes $\{M_3(\mu\text{-}PPh_2)(CO)_9\}_2(\mu_3\text{-}\eta^1,\eta^2,\eta^2{:}\mu_3\text{-}\eta^1,\eta^2,\eta^2\text{-}C_4)$ (M = Ru, Os),[25] and dicobaltcarbonyl complexes of conjugated diynes,[16a,26] polyynes,[27] and *cyclo*-C_{18}[28] (Figure 1). In addition, several complexes have been reported in which a mononuclear tungsten fragment is attached to a triruthenium cluster via a polyyne bridge (Figure 1).[29] Very recently series of related iron and iron−cobalt clusters have also been reported.[30,31]

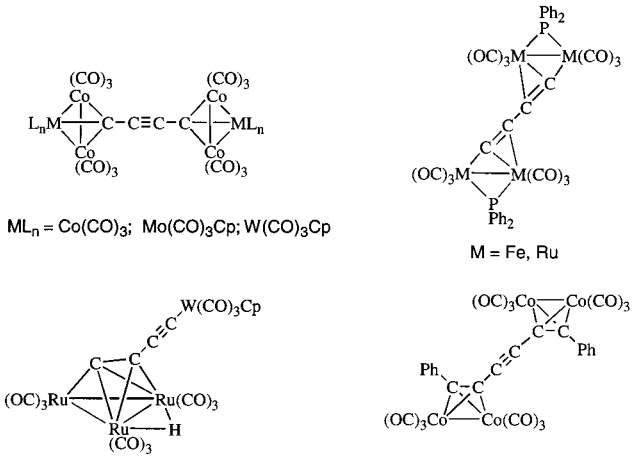

Figure 1. Some representative examples of cluster complexes bearing polyynyl ligands.

However, while the studies described above have shown that strong electronic interactions may occur between two identical metal-based termini through a $(C{\equiv}C)_n$ bridge, evidence for similar interactions between chemically distinct groups remains scarce. Gladysz has described the synthesis of the heterobimetallic complexes $\{Cp^*(NO)(PPh_3)Re\}(\mu\text{-}C{\equiv}C)_n\{PdCl(PEt_3)\}$ (n = 1, 2), which undergo one-electron oxidation processes to yield Re-centered radical cations.[32] The same group has also prepared $Os_3(\mu\text{-}H)[\mu\text{-}\eta^1\text{-}(C{\equiv}C)_n\{Re(NO)(PPh_3)Cp^*\}](CO)_{10}$ (n = 1−3), the structures of which were shown by crystallographic and spectroscopic measurements to contain modest contributions from the $^+Re{=}(C{=}C)_n{=}[Os_3]^-$ resonance form in the ground state.[33] Lapinte and colleagues have shown that the first oxidation of the asymmetrically substituted homometallic complex $\{Cp^*(dppe)Fe\}(\mu\text{-}C{\equiv}CC{\equiv}C)\{Fe(CO)_2Cp^*\}$ results in the formation of a localized Fe(III)−Fe(II) mixed-valence complex.[34]

We have recently described the synthesis and characterization of several carbonyl cluster complexes con-

(15) (a) Osella, D.; Rossetti, R.; Nervi, C.; Ravera, M.; Moretta, M.; Fiedler, J.; Popsisil, L.; Samuel, E. *Organometallics* **1997**, *16*, 695. (b) Osella, D.; Milone, L.; Nervi, C.; Ravera, M. *Eur. J. Inorg. Chem.* **1998**, 1473.

(16) (a) Duffy, N.; McAdam, C. J.; Nervi, C.; Osella, D.; Ravera, M.; Robinson, B. H.; Simpson, J. *Inorg. Chim. Acta* **1996**, *247*, 99. (b) McAdam, C. J.; Duffy, N. W.; Robinson, B. H.; Simpson, J. *Organometallics* **1996**, *15*, 3935. (c) Worth, G. H.; Robinson, B. H.; Simpson, J. *Organometallics* **1992**, *11*, 3863. (d) Dellaca, R. J.; Penfold, B. R.; Robinson, B. H.; Robinson, W. T.; Spencer, J. L. *Inorg. Chem.* **1970**, *9*, 2204.

(17) (a) Frapper, G.; Kertesz, M. *Inorg. Chem.* **1993**, *32*, 732. (b) Belanzoni, P.; Re, N.; Sgamellotti, A.; Floriani, C. *J. Chem. Soc., Dalton Trans.* **1998**, 1825. (c) Re, N.; Sgamellotti, A.; Floriani, C. *J. Chem. Soc., Dalton Trans.* **1998**, 2521. (d) Bruce, M. I.; Halet, J.-F.; Kahlal, S.; Low, P. J.; Skelton, B. W.; White, A. H. *J. Organomet. Chem.*, in press.

(18) (a) Lemoine, P. *Coord. Chem. Rev.* **1982**, *47*, 56. (b) Lemoine, P. *Coord. Chem. Rev.* **1988**, *83*, 169. (c) Geiger, W. E. *Prog. Inorg. Chem.* **1985**, *33*, 275. (d) Drake, S. R. *Polyhedron* **1990**, *9*, 455.

(19) Andres, R. P.; Bielefeld, J. D.; Henderson, J. I.; Janes, D. B.; Kolagunta, V. R.; Kubiak, C. P.; Mahoney, W. J.; Osifchin, R. G. *Science* **1996**, *273*, 1690.

(20) (a) Goh, C.; Holm, R. H. *Inorg. Chim. Acta* **1998**, *270*, 46. (b) Noodleman, L.; Peng, C. Y.; Case, D. A.; Mouesca, J.-M. *Coord. Chem. Rev.* **1995**, *144*, 199. (c) Golbeck, J. H. *Biochim. Biophys. Acta* **1987**, *895*, 167. (d) Cammack, R., Sykes, A. G., Eds. *Iron−Sulfur Proteins*; Academic Press: San Diego, 1992, and references therein.

(21) Akita, M.; Chung, M.-C.; Sakurai, A.; Sugimoto, S.; Terada, M.; Tanaka, M.; Moro-oka, Y. *Organometallics* **1997**, *16*, 4882, and references therein.

(22) Osella, D.; Gambino, O.; Nevi, C.; Ravera, M.; Bertolino, D. *Inorg. Chim. Acta* **1993**, *206*, 155.

(23) Miguel, D.; Moreno, M.; Pérez, J.; Riera, V.; Churchill, D. G.; Churchill, M. R.; Janik, T. S. *J. Am. Chem. Soc.* **1998**, *120*, 417.

(24) (a) Bruce, M. I.; Snow, M. R.; Tiekink, E. R. T.; Williams, M. L. *J. Chem. Soc., Chem. Commun.* **1986**, 701. (b) Adams, C. J.; Bruce, M. I.; Skelton, B. W.; White, A. H. *J. Organomet. Chem.* **1993**, *450*, C9. (c) Blenkiron, P.; Enright, G. D.; Low, P. J.; Corrigan, J. F.; Taylor, N. J.; Chi, Y.; Saillard, J.-Y.; Carty, A. J. *Organometallics* **1998**, *17*, 2447.

(25) Adams, C. J.; Bruce, M. I.; Horn, E.; Skelton, B. W.; Tiekink, E. R. T.; White, A. H. *J. Chem. Soc., Dalton Trans.* **1993**, 3299.

(26) (a) Lewis, J.; Lin, B.; Khan, M. S.; Al-Mandhury, M. R. A.; Raithby, P. R. *J. Organomet. Chem.* **1994**, *484*, 161. (b) Duffy, N.; McAdam, J.; Nervi, C.; Osella, D.; Ravera, M.; Robinson, B.; Simpson, J. *Inorg. Chim. Acta* **1996**, *247*, 99. (c) Bruce, M. I.; Low, P. J.; Werth, A.; Skelton, B. W.; White, A. H. *J. Chem. Soc., Dalton Trans.* **1996**, 1551.

(27) (a) Magnus, P.; Becker, D. P. *J. Chem. Soc., Chem. Commun.* **1985**, 640. (b) Agh-Atabay, N. M.; Lindsell, W. E.; Preston, P. N.; Tomb, P. J.; Lloyd, A. D.; Raugel-Rojo, R.; Spruce, G.; Wherrett, B. S. *J. Mater. Chem.* **1992**, *2*, 1241. (c) Lindsell, W. E.; Preston, P. N.; Tomb, P. J. *J. Organomet. Chem.* **1992**, *439*, 201. (d) Matsumoto, T.; Kotani, S.; Shiina, K.; Sonogashira, K. *Appl. Organomet. Chem.* **1993**, *7*, 613.

(28) Diederich, F.; Rubin, Y.; Chapman, O. L.; Goroff, N. S. *Helv. Chim. Acta* **1994**, *77*, 1441.

(29) (a) Bruce, M. I.; Ke, M.; Low, P. J. *Chem. Commun.* **1996**, 2405. (b) Bruce, M. I.; Skelton, B. W.; White, A. H.; Zaitseva, N. N. *J. Chem. Soc., Dalton Trans.* **1996**, 3151.

(30) Akita, M.; Sakura, A.; Moro-oka, Y. *Chem. Commun.* **1999**, 101.

(31) Akita, M.; Chung, M.-C.; Terada, M.; Miyauti, M.; Tanaka, M.; Moro-oka, Y. *J. Organomet. Chem.* **1998**, *565*, 49.

(32) Weng, W.; Bartik, T.; Brady, M.; Bartik, B.; Ramsden, J. A.; Arif, A. M.; Gladysz, J. A. *J. Am. Chem. Soc.* **1995**, *117*, 11922.

(33) Falloon, S. B.; Szafert, S.; Arif, A. M.; Gladysz, J. A. *Chem. Eur. J.* **1998**, *4*, 1033.

(34) Coat, F.; Guillevic, M.-A.; Toupet, L.; Paul, F.; Lapinte, C. *Organometallics* **1997**, *16*, 5988.

taining metallocarbon cores with various polyhedral geometries bearing pendant trimethylsilylacetylene ligands.[35] As the trimethylsilyl acetylene moiety is a protected form of the terminal acetylene functional group, C≡CH, which is in turn a traditional source of metal acetylide complexes, it is our contention that these metallocarbon clusters will prove to be viable reagents in the synthesis of electronically interesting heterometallic materials and molecular networks through a combination of deprotection, oxidative coupling, and metalation reactions as well as the direct attachment of other substrates.

In this paper, we describe the preparation of two complexes that contain a mononuclear $Cp(PPh_3)_2Ru$ metal fragment and a dicobalt−dicarbon cluster core linked via acetylene-based bridging ligands. The spectroscopic and electrochemical properties of these compounds not only demonstrate that significant electronic interactions may be observed between vastly different metal fragments but also indicate that subtle changes in the nature of the bridging ligands may allow the optical properties of these species to be tuned. A detailed theoretical study utilizing DFT, ZINDO, and ELF methods has been undertaken to provide an orbital-based rationalization of the observed properties.

Results and Discussion

Syntheses. The synthetic and reaction chemistry associated with alkyne−dicobalt carbonyl complexes has been extensively examined over a period of many years, and these compounds have found widespread application in preparative organic chemistry.[36−38] As a result, $Co_2(CO)_6$ complexes of a great many alkyne reagents have been prepared, and their structures and reactivity examined.[39] Reaction of the hexacarbonyl Co_2−alkyne complexes with phosphines or phosphites under relatively mild thermal conditions leads to CO substitution and formation of complexes of general form $Co_2(\mu\text{-}\eta^2\text{-}RC_2R)(CO)_{6-n}L_n$.[26a,28,39] Of particular relevance to the current study is the observation that substitution of two carbonyl ligands by bis(diphenylphosphino)methane (dppm) affords complexes of increased stability which display a simplified electrochemical response (vide infra).[16b]

Conjugated 1,3-diynes have also been shown to undergo reaction with $Co_2(CO)_8$, affording complexes in which one or both C≡C triple bonds are coordinated according to the stoichiometry of the reaction.[16a,26,39] Given the synthetic challenges associated with the preparation of more highly conjugated polyynes (1,3,5-triynes, 1,3,5,7-tetraynes, etc.), it is not surprising that the reactions of $Co_2(CO)_8$ with these species have been much less extensively investigated. The Diederich group examined the 1:1 reaction of $Co_2(CO)_8$ with 1,6-bis(triisopropylsilyl)hexa-1,3,5-triyne and found exclusive formation of $Co_2(\mu\text{-}\eta^2\text{-}Pr^i_3SiC{\equiv}CC_2C{\equiv}CSiPr^i_3)(CO)_6$, in which the cobalt carbonyl fragment was coordinated to the central carbon−carbon triple bond, which was attributed to the presence of the bulky triisopropylsilyl end-caps.[28] A bis(dicobalt) complex of 1,8-bis(trimethylsilyl)octa-1,3,5,7-tetrayne prepared by oxidative coupling of a diyyne precursor was also described. Lewis et al. have made a similar observation.[26a]

Scheme 1[a]

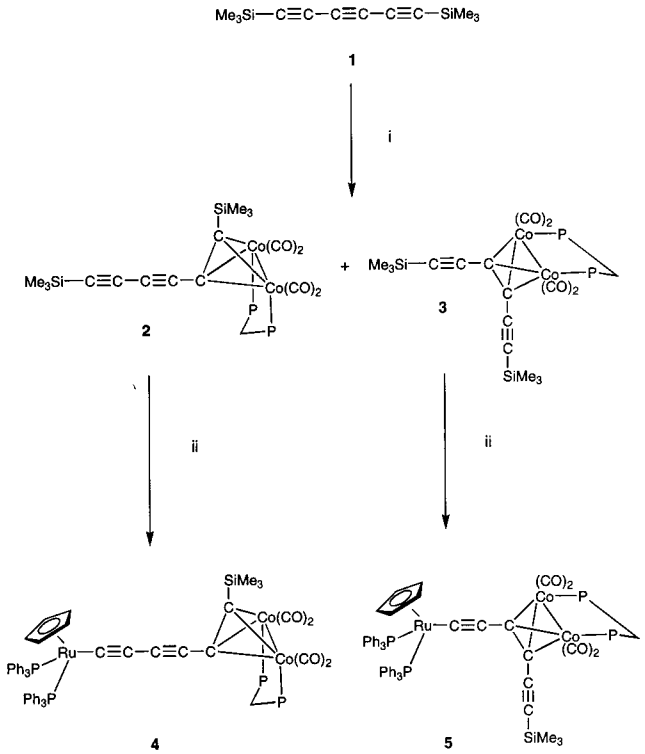

[a] (i) $Co_2(CO)_6$(dppm)/benzene/80 °C. (ii) $RuCl(PPh_3)_2Cp$/KF/MeOH/60 °C.

We were interested in preparing $Co_2(CO)_4$(dppm)−triyne derivatives with a dicobalt moiety coordinated to either the terminal or central alkyne moiety for use as redox-active polycarbon ligands. We chose to examine the reaction between $Co_2(CO)_6$(dppm) and 1,6-bis(trimethylsilyl)hexa-1,3,5-triyne $Me_3SiC{\equiv}CC{\equiv}CC{\equiv}CSiMe_3$ (**1**) on the basis that the relatively sterically undemanding $SiMe_3$ end-caps might permit coordination of the dicobalt reagent not only to the central alkyne fragment but also to the terminal C≡C moieties.

The reaction of $Co_2(CO)_6$(dppm) with **1** in refluxing benzene afforded two dark red crystalline complexes $Co_2(\mu\text{-}Me_3SiC_2C{\equiv}CC{\equiv}CSiMe_3)(CO)_4$(dppm) (**2**) (15%) and $Co_2(\mu\text{-}Me_3SiC{\equiv}CC_2C{\equiv}CSiMe_3)(CO)_4$(dppm) (**3**) (42%), which were readily separated by chromatography on silica gel (Scheme 1). The steric bulk of the dppm ligand is sufficient to prevent serendipitous coordination of two Co_2 fragments to one molecule of **1**, but insufficient to

(35) (a) Low, P. J.; Enright, G. D.; Carty, A. J. *J. Organomet. Chem.* **1998**, *565*, 279. (b) Low, P. J.; Udachin, K. A.; Enright, G. D.; Carty, A. J. *J. Organomet. Chem.* **1999**, *578*, 103.

(36) (a) Davies, S. G. In *Organotransition Metal Chemistry: Applications to Organic Synthesis*; Pergamon: Oxford, 1986; pp 86−90. (b) Kunz, H.; Waldmann, H. In *Comprehensive Organometallic Chemistry II*; Abel, E. W., Stone, F. G. A., Wilkinson, G., Eds.; Elsevier: New York, 1995; Vol. 6, pp 692−693.

(37) (a) Pauson, P. L. In *Organometallics in Organic Synthesis*; de Meijere, A. tom Dieck, H., Eds.; Springer-Verlag: Berlin, 1987; pp 233−246. (b) Shore, N. E. *Chem. Rev.* **1988**, *88*, 1081. (c) Shore, N. E. In *Comprehensive Organic Synthesis*; Trost, B. M., Flemming, I., Eds.; Pergamon: Oxford, 1991; Vol. 5, pp 1037−1064. (d) Shore, N. E. In *Comprehensive Organometallic Chemistry II*; Abel, E. W., Stone, F. G. A., Wilkinson, G., Eds.; Elsevier: New York, 1995; Vol. 12, pp 703−739.

(38) (a) Nicholas, K. M. *Acc. Chem. Res.* **1987**, *20*, 207. (b) Caffyn, A. J. M.; Nicholas, K. M. In *Comprehensive Organometallic Chemistry II*; Abel, E. W., Stone, F. G. A., Wilkinson, G., Eds.; Elsevier: New York, 1995; Vol. 12, pp 685−702. (c) Vizniowski, C. S.; Green, J. R.; Breen, T. L.; Dalacu, A. V. *J. Org. Chem.* **1995**, *60*, 7496.

(39) For a review of Co_2(alkyne) complexes see: Dickson, R. S.; Fraser, P. J. *Adv. Organomet. Chem.* **1974**, *12*, 323.

completely restrict coordination to the alkyne moiety adjacent to an $SiMe_3$ group.

The compounds **2** and **3** were characterized by the usual spectroscopic methods and microanalytical data and the structures confirmed by a single-crystal X-ray study in each case (vide infra). The inequivalent $SiMe_3$ groups in **2** give rise to distinct resonances at δ_H 0.31, 0.37 and δ_C 0.87, 1.57. The ^{13}C NMR spectrum also contains a triplet resonance at δ_C 37.99 (J_{CP} = 20 Hz) for the dppm methylene carbon. The carbon centers of the Co_2C_2 cluster core give rise to triplet resonances at δ_C 75.41 (J_{CP} = 8 Hz) and 82.39 (J_{CP} = 4 Hz), while the remaining carbon nuclei of the polyyne chain are observed as singlets at δ_C 81.48, 91.34, 91.55, and 92.89. In contrast, single $SiMe_3$ resonances are observed at δ_H 0.29 and δ_C 0.44 for the symmetrical isomer **3**. The identical carbon centers of the tetrahedral cluster core produced a single broad resonance at δ_C 70.37, while singlet resonances at δ_C 103.27 and 107.85 are assigned to the carbon centers of the pendant ethynyl moieties. Mass spectra of **2** and **3**, obtained using fast atom bombardment (FAB) ionization techniques, show $[M-nCO]^+$ ions (n = 1−4) in each case.

The many examples of known cobalt−carbonyl alkyne complexes render **2** and **3**, by themselves, rather unremarkable. However, from our perspective, the interest in these complexes comes from the presence of the pendant, wirelike trimethylsilyl-capped alkynyl (**2**) and diynyl (**3**) groups that are attached directly to the electrochemically active Co_2C_2 core.

Recently, several reports have described the synthesis of Fe(II) and Ru(II) acetylide complexes from trialkylsilyl-substituted alkynes and an appropriate metal substrate in the presence of a source of the fluoride ion.[14,40] The application of similar reaction conditions to a mixture of $RuCl(PPh_3)_2Cp$ and one of the $Co_2(CO)_4$(dppm)-substituted hexatriynes **2** or **3** afforded good yields of the complexes $Co_2\{\mu$-$Me_3SiC_2C{\equiv}CC{\equiv}C[Ru(PPh_3)_2Cp]\}(CO)_4$(dppm) (**4**) and $Co_2\{\mu$-$Me_3SiC{\equiv}CC_2C{\equiv}C[Ru(PPh_3)_2Cp]\}(CO)_4$(dppm) (**5**), respectively (Scheme 1).

Thus, treatment of **2** with 1 equiv of $RuCl(PPh_3)_2Cp$ and 1.5 equiv of KF in a thf/methanol mixture (1:1) gave the reddish brown diynyl complex $Co_2\{\mu$-$Me_3SiC_2C{\equiv}CC{\equiv}C[Ru(PPh_3)_2Cp]\}(CO)_4$(dppm) (**4**) in good (79%) yield. The ^1H and ^{13}C NMR spectra contained the anticipated resonances for the $SiMe_3$ (δ_H 0.78, δ_C 1.21) and Cp (δ_H 4.55, δ_C 86.41) ligands. The retention of the $SiMe_3$ group attached adjacent to the cluster core in **4** is perhaps not too surprising, as cleavage of the Co_2C_2−$SiMe_3$ bond is known to require somewhat more forcing conditions than the corresponding ≡C−$SiMe_3$ bond.[26a,28,41] A triplet resonance at δ_C 36.82 is readily assigned to the methylene group of the dppm ligand, although in the proton spectrum only a broad, unresolved signal (δ_H 3.43) is observed, suggesting that at room temperature the methylene group oscillates between the endo and exo positions. Six low-intensity signals are assigned to the carbon centers in the Co_2C_2 cluster core [C(5/6) δ_C 84.68 (t, J_{CP} = 9 Hz), 89.72 (t, J_{CP} = 5 Hz)] and the remainder of the polycarbon ligand [C(1) δ_C 90.09 (t, J_{CP} = 16 Hz), C(2) δ_C 100.08, C(3) δ_C 89.82 and C(4) δ_C 64.69 (br)] by comparison of the J_{CP} and chemical shift values with those of **2**. The atom-numbering scheme used to describe the NMR spectra of **2**−**5** follows that given in the appropriate ORTEP figure. The FAB mass spectrum is characterized by an $[M+H]^+$ ion at m/z 1450, which fragmented by competitive loss of CO and PPh_3 ligands to give $[M-nCO]^+$ (n = 1−4) and $[M-nCO-mPPh_3]^+$ (m = 1, 2; n = 0, 3, 4) daughter ions.

A similar reaction between **3** and $RuCl(PPh_3)_2Cp$, also in the presence of KF, gave the strikingly green-colored complex $Co_2\{\mu$-$Me_3SiC{\equiv}CC_2C{\equiv}C[Ru(PPh_3)_2Cp]\}(CO)_4$(dppm) (**5**) (74%). Substitution of only one $SiMe_3$ group in **3** by an $Ru(PPh_3)_2Cp$ fragment is indicated by the NMR data, with both $SiMe_3$ (δ_H 0.47, δ_C 1.035) and Cp (δ_H 4.55, δ_C 86.61) resonances being detected along with those of the dppm (δ_H 3.79, 3.10; δ_C 34.52) ligand. Other ^{13}C resonances are assigned to C(1) [δ_C 111.08 (t, J_{CP} = 4 Hz)], C(2) 114.78, C(5) and C(6) [δ_C 99.75, 95.78]. The cluster-bound C(3) and C(4) nuclei were not detected. The FAB-MS is similar to that of **4** and contains $[M+H]^+$ as the highest molecular weight ion, with fragment ions derived from loss of both CO and PPh_3 ligands. Rather surprisingly, the remaining ≡C−$SiMe_3$ bond in **5** has proven to be remarkably robust, and there was no evidence for the formation of the corresponding desilylated product, $Co_2\{\mu$-$HC{\equiv}CC_2C{\equiv}C[Ru(PPh_3)_2Cp]\}(CO)_4$(dppm), even in the presence of a large excess of KF.

The resistance of the remaining ≡C−$SiMe_3$ group in **5** to fluoride ion (i.e., nucleophile) induced cleavage remains a curiosity at this stage. It may be that the electron-rich $Ru(PPh_3)_2Cp$ group induces a small, but significant, increase in electron density at the silicon center through the cluster-spaced bridging ligand, thereby reducing the susceptibility of this group to nucleophilic attack.

Molecular Structures. Single-crystal X-ray diffraction studies were carried out on each of complexes **2**, **3**, **4**, and **5** in order to examine the structural variation within the series. Crystallographic details are collected in Table 1, while important bond lengths and angles are summarized in Table 2. ORTEP plots indicating the atom-labeling schemes are given in Figures 2 (**2**), 3 (**3**), 4 (**4**), and 5 (**5**).

An examination of the structure of complex **2** shows a chain of four carbon atoms [C(1−4)] with the typical short, long, short, long bond length alternation associated with a diyne moiety. The [C(1−4)] four carbon fragment is essentially linear, with the greatest deviation from linearity being found at C(1). The C(1) end of the chain is capped by the Si(1) trimethylsilyl group, while C(4) is connected to the tetrahedral Co_2C_2 metallocarbon core via C(5). The Co(1)−Co(2) separation is 2.476(2) Å, which may be considered typical for this type of cluster.[26a,c] Both Co centers are further connected to C(5) [Co(1,2)−C(5) 1.964(8), 1.973(8) Å] and C(6) [Co(1,2)−C(6) 1.963(7), 1.977(7) Å]. Two carbonyl ligands and a phosphine from the dppm ligand complete the coordination geometry about each Co center. Treating Co(1)−Co(2)−C(6) as the basal plane of the Co_2C_2 tetrahedron, the bidentate dppm ligand occupies the two available pseudoequatorial positions. A connection be-

(40) (a) Lomprey, J. R.; Selegue, J. P. *Organometallics* **1993**, *12*, 616. (b) Weyland, T.; Lapinte, C.; Frapper, G.; Calhorda, M. J.; Halet, J.-F.; Toupet, L. *Organometallics* **1997**, *16*, 2024. (c) Bruce, M. I.; Hall, B. C.; Kelly, B. D.; Low, P. J. Unpublished results.

(41) Bruce, M. I.; Low, P. J.; Werth, A.; Skelton, B. W.; White, A. H. *J. Chem. Soc., Dalton Trans.* **1996**, 1551.

Table 1. Summary of Crystallographic Data for 2−5

	2	3	4	5
formula	$C_{41}H_{40}Co_2O_4P_2Si_2$	$C_{41}H_{40}Co_2O_4P_2Si_2$	$C_{79}H_{66}Co_2O_4P_4RuSi.0.5C_6H_{14}$	$C_{79}H_{66}Co_2O_4P_4RuSi.2C_3H_6O$
fw	832.74	832.74	1493.37	1566.44
crystal size (mm)	0.15 × 0.10 × 0.03	0.30 × 0.30 × 0.30	0.20 × 0.10 × 0.01	0.20 × 0.20 × 0.30
crystal system	monoclinic	triclinic	monoclinic	triclinic
space group	$P2_1/c$	$P\bar{1}$	$P2_1/c$	$P\bar{1}$
a, Å	12.177(1)	11.2289(5)	18.436(1)	12.314(6)
b, Å	23.160(3)	11.7570(5)	25.607(2)	15.3649(7)
c, Å	29.993(3)	16.6934(8)	17.349(1)	22.370(1)
α, deg	90	95.01(1)	90	96.00 (1)
β, deg	91.86(3)	91.67(1)	111.40(2)	104.08(1)
γ, deg	90	106.84(1)	90	106.53(1)
V, Å^3	8454(1)	2097.8(2)	7625(1)	3866.5(3)
Z	8	2	4	2
D_c, g.cm^{-3}	1.308	1.318	1.301	1.345
F(000)	3440	860	3076	1616
μ, mm^{-1}	0.954	0.962	0.773	0.767
2θ range, deg	2.72−45	2.46−57.46	4.34−50	2.82−57.46
no. of reflns measd	58380	25025	47221	45969
no. of unique reflns	10754	10776	13171	19845
no. of obsd reflns	4550	7818	8197	14512
no. of params refined	972	461	880	878
final *R*, R_w	0.0789, 0.0689	0.0425, 0.0851	0.0511, 0.1003	0.0389, 0.0885
GOF	0.902	0.900	0.893	1.015
max, min residual density, e Å^{-3}	+0.370, −0.392	+0.945, −0.659	+0.689, −0.464	+0.610, −0.681

Table 2. Selected Bond Lengths (Å) and Angles (deg) for Complexes 2, 3, 4, 5, and Ru(C≡CPh)(PPh$_3$)$_2$Cp (6)

	2	3	4	5	6[f]
Co(1)−Co(2)	2.476 (2)	2.4684(4)	2.4856(8)	2.4763(5)	
Co(1)−C(5)	1.964(8)	1.958(2)[a]	1.979(4)	1.954(2)[a]	
Co(1)−C(6)	1.963(7)	1.964 (2)[b]	1.966(4)	1.981(2)[b]	
Co(2)−C(5)	1.973(8)	1.954(2)[a]	1.970(4)	1.964(2)[a]	
Co(2)−C(6)	1.977(7)	1.951 (2)[b]	1.979(4)	1.965(2)[b]	
Co(1)−P(1)	2.223(2)	2.2387(6)	2.209(1)	2.2315(6)	
Co(2)−P(2)	2.213(2)	2.2217(6)	2.220 (1)	2.2277(7)	
Co(1)−C(13)	1.77(1)	1.784(2)	1.777(6)	1.773(3)	
Co(1)−C(14)	1.799(10)	1.786(2)	1.789(6)	1.774(3)	
Co(2)−C(15)	1.814(10)	1.796(2)	1.796(5)	1.786(3)	
Co(2)−C(16)	1.779(10)	1.783(2)	1.758(6)	1.778(3)	
C−O(av)	1.147	1.138	1.136	1.142	
Si(1)−C(1)	1.86(1)	1.843(2)		1.830(3)	
C(1)−C(2)	1.19 (1)	1.208(3)	1.230(6)	1.211(3)	1.214(7)
C(2)−C(3)	1.37 (1)	1.409(3)	1.359(6)	1.407(3)	
C(3)−C(4)	1.203(10)	1.367(3)	1.219(6)	1.370(3)	
C(4)−C(5)	1.398(10)	1.402(3)	1.382(6)	1.395(3)	
C(5)−C(6)	1.376(9)	1.201(3)	1.361(6)	1.217(3)	
C(1)−Si(2)	1.847(7)	1.841(2)	1.831(5)		
Ru(1)−C(1)			1.981(4)	1.997(2)[c]	2.017(5)
Ru(1)−P(3)			2.297 (1)	2.2855(7)	2.229(3)
Ru(1)−P(4)			2.296 (1)	2.2836(7)	2.228(3)
Ru(1)−Cp(av)			2.232	2.239	2.239
Si(1)−C(1)−C(2)	175(2)	177.8 (2)	171.9(4)[d]	175.7(2)	
C(1)−C(2)−C(3)	176.7(17)	174.6(2)	178.7(5)	176.7(2)	
C(2)−C(3)−C(4)	176.8(9)	140.2(2)	178.1(5)	138.6(2)	
C(3)−C(4)−C(5)	177.4(9)	139.5(2)	176.2(5)	143.9(2)	
C(4)−C(5)−C(6)	141.6(8)	178.1(2)	140.5(4)	176.1(2)	
C(5)−C(6)−Si(2)	138.7(6)	176.9(2)	141.6(3)	178.0(2)[e]	
P(3)−Ru(1)−P(4)			103.73(5)	102.08(2)	100.9(1)

[a] Read C(3) for C(5). [b] Read C(4) for C(6). [c] Read C(6) for C(1). [d] Read Ru(1) for Si(1). [e] Read Ru(1) for Si(2). [f] Reference 42.

tween C(6) and Si(2) [1.847(7) Å] completes the coordination about the metallocarbon cluster core.

Figure 3 clearly shows that complex **3** is a simple structural isomer of **2**, in which the Co_2 group has coordinated to the central C(3)−C(4) C≡C group in **1**. The C(1)−C(2) and C(5)−C(6) separations are characteristic of alkyne moieties and are equivalent, within error, at 1.208(3) and 1.201(3) Å, respectively. Overall, the dimensions of the Co_2C_2 core in **2** appear to be somewhat greater than in **3**. Since these molecules contain a cluster-based HOMO which is bonding in nature (vide infra), this discrepancy may be due to the greater electron-donating character of $SiMe_3$ (**2**) when measured against C≡C$SiMe_3$ (**3**). In keeping with this notion, it may also be noted that the average C−O bond distance in **2** [1.147 Å] is greater than in **3** [1.138 Å]. The expansion of the Co_2C_2 core in **2** relative to that in **3** may also be enhanced by the shorter and stronger Co−P bonds in **2** (Co−P av 2.218 Å **2**; 2.231 Å **3**).

Figure 4 shows that complex **4** is derived from **2** by substitution of the Si(1)Me_3 group by a Ru(PPh_3)$_2$Cp fragment. In general the structural parameters of the common fragments are the same, within experimental error. However, the following trends are worth noting.

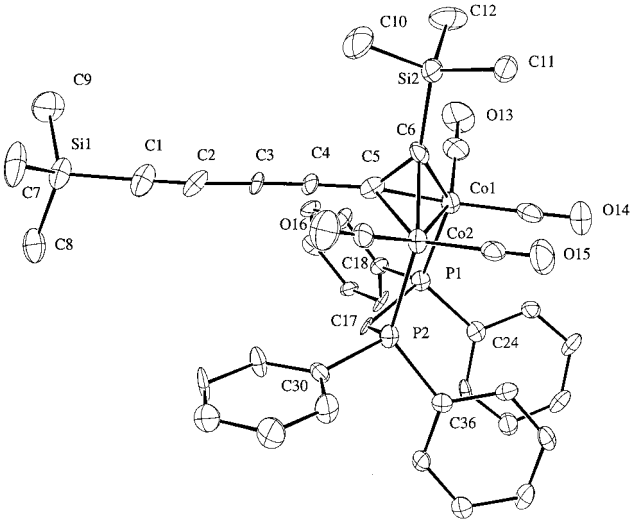

Figure 2. Molecular structure of **2** indicating the atom-labeling scheme. Thermal ellipsoids in this and all subsequent figures are drawn at the 30% probability level.

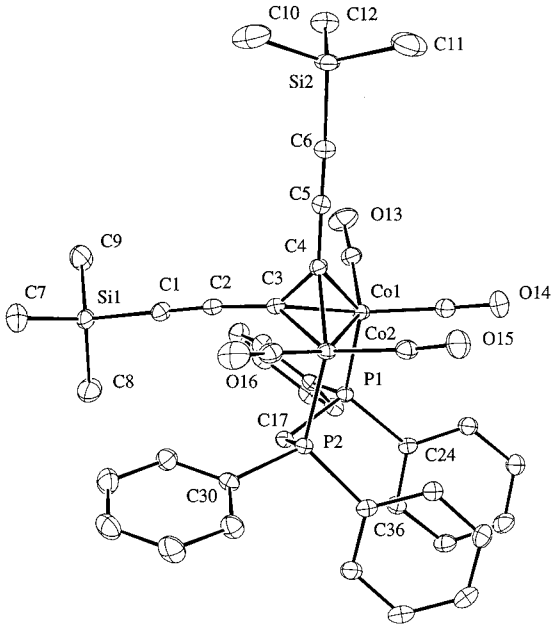

Figure 3. Molecular structure of **3** indicating the atom-labeling scheme.

Within the C(1−4) diyne moiety, the separations of the triple-bonded carbons C(1)−C(2) and C(3)−C(4) are greater in **4** than **2** [1.230(6), 1.219(6) Å (**4**) vs 1.19(1), 1.20(1) Å (**2**)], while the C−C single bonds C(2)−C(3) and C(4)−C(5) are shorter [1.359(6), 1.382(6) Å (**4**) vs 1.37(1), 1.40(1) Å (**2**)]. On average, there is an increase in the dimensions of the Co(1)−Co(2)−C(5)−C(6) cluster core in **4** when compared to **2**.

When the bonding parameters of the mononuclear ruthenium fragment are compared with the corresponding data from the prototypical acetylide complex Ru(C≡CPh)(PPh_3)$_2$Cp (**6**), some further trends become apparent (Table 2).[42] The Ru(1)−C(1) distance in **4** is shorter than in **6**, while the opposite is true for the C(1)−C(2) distance. The Ru−P separations in the heterometallic complex **4** are significantly elongated in comparison to those in **6**. Similar structural trends were noted between **6** and Ru(C≡C$C_6H_4NO_2$-*p*)(PPh_3)$_2$Cp.[42b]

(42) (a) Bruce, M. I.; Humphrey, M. G.; Snow, M. R.; Tiekink, E. R. T. *J. Organomet. Chem.* **1986**, *314*, 213. (b) Whittall, I. R.; Humphrey, M. G.; Persoons, A.; Houbrechts, S. *Organometallics* **1996**, *15*, 1935.

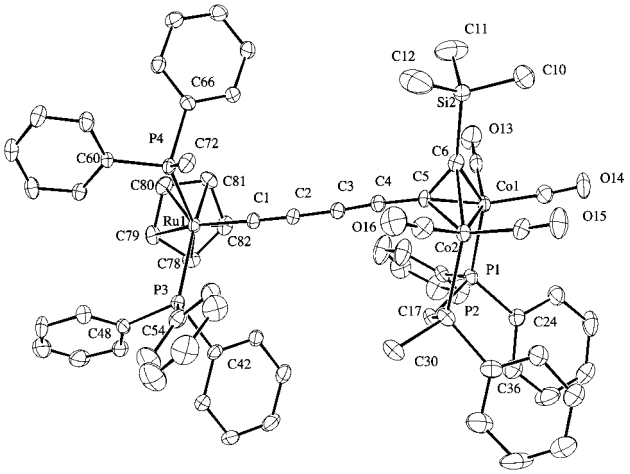

Figure 4. Molecular structure of **4** indicating the atom-labeling scheme. Only the *ipso*-carbons of the C(30)−C(35) and C(72)−C(77) phenyl groups are shown for clarity.

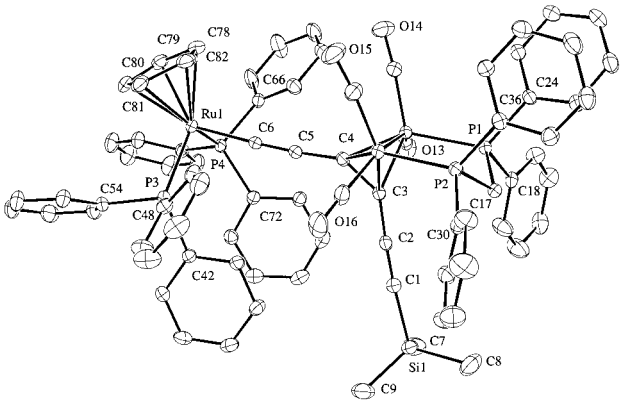

Figure 5. Molecular structure of **5** indicating the atom-labeling scheme.

A molecule of complex **5** is illustrated in Figure 5. The mononuclear fragment has substituted the $SiMe_3$ moiety attached at C(6), on the opposite side of the Co(1,2)−C(3,4) cluster to the dppm ligand, a fact that can be attributed to steric influences. Similar trends are apparent between **3** and **5** as has been indicated for **2** and **4,** notably that the dimensions of the Co_2C_2 cluster core in **5** are greater than found in **3**. The mononuclear fragment in **5** is almost identical with that of the comparable fragment in **4**, and therefore as noted above for **4** the Ru(1)−P(3,4) separations are longer than in **6**. The ≡C(1)−Si(1) bond is the shortest in this series at 1.830(3) Å, a fact that may be related to the surprising resilience of this bond toward cleavage (vide supra).

In summary, there is some indication that for both **4** and **5** the mononuclear fragment donates electron density through the carbon bridging ligand to the Co_2C_2 cluster core, which expands as a result. The increased electron density at the cluster core is then relieved to a certain extent through π-back-bonding into the carbonyl ligands. However, for the Ru−C and C−C distances these trends are at the borderline of statistical significance, and it should be noted that the bonding parameters of acetylenic linkages are notoriously insensitive to electronic effects.[8b]

Table 3. IR and UV−Vis Data for Complexes 2, 3, 4, and 5 (ν in cm^{-1}, ϵ in $cm^{-1}\ M^{-1}$)

	ν(C≡C)[a]	ν(CO)[a]	UV/vis abs (ϵ)[b]
2	2160	2030vs, 2009vs, 2004sh, 1982vs, 1962w	216 (72500), 278 (34060), 354 (10690), 448 (1532), 548 (1050)
3	2118, 2105	2037vs, 2019vs, 1994vs, 1972w	218 (85000), 288 (36560), 354 (14000), 446 (1587), 542 (1160)
4	2124	2018s, 1998vs, 1970vs, 1952w	214 (105840), 294 (44520), 348 (32400), 572 (1703)
5	2104	2036s, 2015sh, 2000vs, 1975vs, 1954w	220 (134,700), 268 (61530), 358 (45400), 600 (2300)

[a] Measured in cyclohexane. [b] Measured in thf.

Infrared Spectra. The ν(CO) spectrum of each complex **2**, **3**, **4**, and **5** is characterized by a pattern of three strong bands and other much weaker features (Table 3). The conjugated C≡C moieties in **2** give rise to a single ν(C≡C) band at 2160 cm^{-1}. In the case of the "V"-shaped molecule **3**, both the symmetric and antisymmetric vibrations result in an oscillation of the molecular dipole moment. Consequently both modes are IR active and two absorption bands are observed (2118, 2105 cm^{-1}).

The spectra of the heterometallic complexes **3** and **4** display a pattern of ν(CO) bands similar to that found in the precursors **2** and **3**. For **4** however only a single ν(C≡C) band was observed. On average, the ν(CO) bands of **4** are shifted to lower energy by ca. 10 cm^{-1} when compared with the parent complex **2**. In **5**, the highest energy A_1 ν(CO) band (2036 cm^{-1}) is broader and less intense than the corresponding band in **3**. The other strong ν(CO) bands in **5** appear at lower frequencies than the analogous bands in the precursor. The decrease in the frequency of the ν(CO) bands in the heterometallic complexes **4** and **5** relative to **2** and **3** suggests an increase in the electron density at the Co_2C_2 core in these compounds following substitution of an $SiMe_3$ group by the electron-rich $Ru(PPh_3)_2Cp$ fragment. A decrease in the ν(C≡C) band of 36 cm^{-1} in **4** compared to **2** is consistent with a small decrease in the C≡C bond strength in this complex.

UV−Vis Spectra. The most visually apparent distinction between the complexes **2**−**5** is the color, which ranges from dark red (**2** and **3**) through green-brown (**4**) to striking dark green (**5**), prompting an examination of the UV−vis spectra across the series.

The spectra of **2** and **3** closely resemble that of the protio derivative $Co_2(\mu\text{-}\eta^2\text{-}HC{\equiv}CC_2C{\equiv}CH)(CO)_4(dppm)$,[28] and a series of weak, overlapping d−d bands are observed in the visible region (Figure 6, Table 3). In the case of **4** and **5** bands at 572 nm (**4**) and 600 nm (**5**) dominate the visible region, which account for the color of these complexes (Figure 6). This band displays modest solvatochromatic behavior, with a shift in λ_{max} of 12 nm found for **5** in cyclohexane and dimethylformamide. It would therefore appear more likely that these visible absorption bands in **4** and **5** are d−d in origin rather than $Ru-Co_2C_2$ charge-transfer transitions.

The Ru-containing complexes also displayed MLCT bands at 348 nm (**4**) and 358 nm (**5**). Similar MLCT bands have been noted for a series of related Ru−acetylide complexes $Ru(C{\equiv}CC_6H_4R)(PR'_3)_2Cp$.[42] The energy of these bands decreased upon substitution of R = H [λ_{max} 306 nm (cyclohexane)] for R = NO_2 [λ_{max} 437 nm (cyclohexane)], a fact that was attributed to the increased stabilization of the charge-separated form in the nitro-substituted derivative. In each complex **2**−**5** an intense absorption, presumably arising from $\pi-\pi^*$ transitions in the Ph groups of the dppm ligand, is observed at highest energy in the UV region (Table 3).

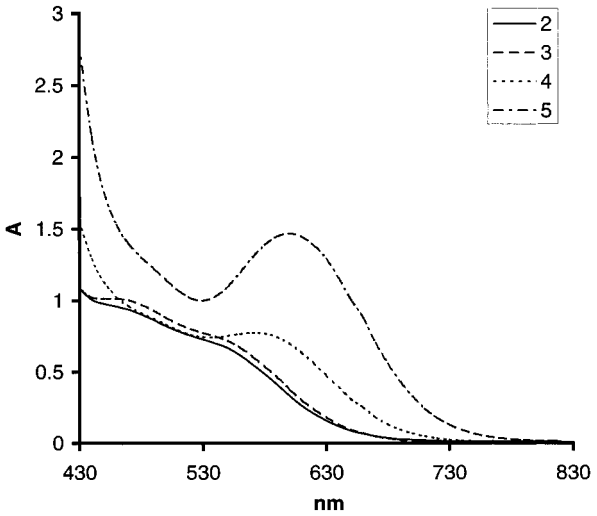

Figure 6. Visible spectra of complexes **2**−**5** in thf (6.5×10^{-4} M).

Electrochemistry. The hexacarbonyl complexes $Co_2(alkyne)(CO)_6$ undergo one-electron, diffusion-controlled reduction processes, followed by a series of fast chemical reactions which lead to Co−Co bond rupture and/or loss of a $Co_2(CO)_6$ fragment.[26a] The net result is rapid decomposition of the radical anions $[Co_2(alkyne)(CO)_6]^{\bullet-}$ at room temperature. Chemical reversibility of the electrochemical process is improved by the presence of electron-withdrawing or bulky substituents on the alkyne.[43] Oxidation processes have not been observed for the hexacarbonyl compounds within the potential windows examined.[44]

However, in the case of the substituted derivatives $Co_2(RC_2R')(CO)_{6-n}(L)_n$ [n = 1−3, L = $P(OMe_3)$; n = 2,4 L_2 = dppm] the Co_2C_2 core was found to be sufficiently electron rich to be oxidized at readily accessible potentials in CH_2Cl_2.[16b,43b] For the dppm derivatives, the oxidation process is reversible, a trait that has been attributed to stabilization of the Co−Co bond by the bridging bisphosphine ligand, although fast chemical complications were reported to hamper the study of the reduction process in these complexes.[43b] Mononuclear acetylide complexes containing electron-rich metal centers are well-known to undergo one-electron oxidation processes to give 17e radical cations $[L_nM-C{\equiv}CR]^{\bullet+}$,[45] the stability of which depends greatly on the steric bulk of the supporting ligands.[13a,46]

(43) (a) Osella, D.; Fiedler, J. *Organometallics* **1992**, *11*, 3875. (b) Duffy, N. W.; McAdam, C. J.; Robinson, B. H.; Simpson, J. *J. Organomet. Chem.* **1998**, *565*, 19.

(44) Arewgoda, C. M.; Robinson, B. H.; Simpson, J. *J. Am. Chem. Soc.* **1983**, *105*, 1893.

(45) (a) Connelly, N. G.; Gamasa, M. P.; Gimeno, J.; Lapinte, C.; Lastra, E.; Maher, J. P.; Le Narvor, N.; Rieger, A. L.; Rieger, P. H. *J. Chem. Soc., Dalton Trans.* **1993**, 2575. (b) Adams, J. S.; Bitcon, C.; Brown, J. R.; Collison, D.; Cunningham, M.; Whiteley, M. W. *J. Chem. Soc., Dalton Trans.* **1987**, 3049. (c) Beddoes, R. L.; Bitcon, C.; Whiteley, M. W. *J. Organomet. Chem.* **1991**, *402*, 85. (d) Whittall, I. R.; Humphrey, M. G.; Hockless, D. C. R.; Skelton, B. W.; White, A. H. *Organometallics* **1995**, *14*, 3970.

Table 4. Cyclic Voltammetry Data[a]

	$E_{Red}°$ (i_pa/i_pc) [ΔE_p]	$E_{Ox1}°$ (i_pa/i_pc) [ΔE_p]	$E_{Ox2}°$ [ΔE_p]
2	−1.09 (1.0) [0.33]	1.49 (1.0) [0.35]	
3	−1.06 (1.0) [0.36]	1.60 (1.0) [0.38]	
4	−1.29 (1.0) [0.31]	0.96 (0.87)[b] [0.30]	1.16 [0.27]
5	−1.36 (1.0) [0.29]	0.86 (0.93)[b] [0.29]	1.14 [0.30]

[a] All data collected from thf solutions containing 0.05 M [$^nBu_4N$]BF_4 as supporting electrolyte, at −50 °C, scan rate 100 mV s^{-1}, analyte concentration 1×10^{-3}, Pt disk working electrode, Ag wire pseudo reference, Pt wire counter electrode. Internal Fc/Fc^+ reference at $E°$ 0.99V, i_pa/i_pc, ΔE_p 0.38 V. [b] Measured from the isolated wave.

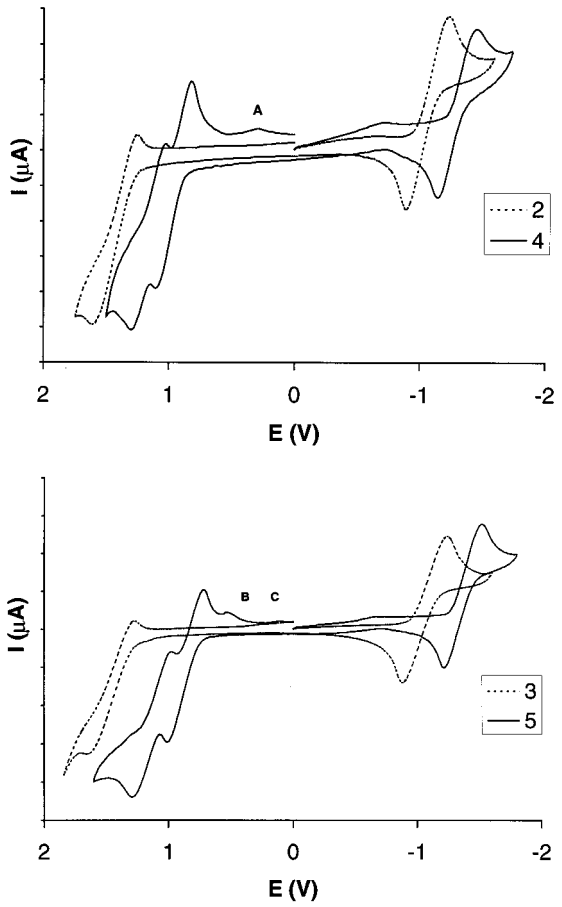

Figure 7. Cyclic voltammograms of (a) **2** and **4** and (b) **3** and **5**.

The presence of both of these types of redox-active site encouraged an examination of the electrochemical response of **2**−**5**, using cyclic votammetry techniques. The results obtained are gathered in Table 4. In thf solvent at −50 °C the parent cobalt−carbon clusters **2** and **3** have reversible one-electron oxidation and reduction waves, corresponding to the formation of the radical cations $[\mathbf{2}]^{\bullet+}$ ($E_{Ox1}°$ +1.49 V) and $[\mathbf{3}]^{\bullet+}$ ($E_{Ox1}°$ +1.60 V) and radical anions $[\mathbf{2}]^{\bullet-}$ ($E_{Red}°$ −1.09 V) and $[\mathbf{3}]^{\bullet-}$ ($E_{Red}°$ −1.06 V), respectively (Figure 7). Peak to peak separations for each process are comparable to that of the ferrocene/ferrocenium couple under identical conditions, and the i_{pa}/i_{pc} ratio in each case is unity. Linear plots of i_{pa} against the square of the scan rate were also obtained. As indicated above, a similar electrochemical response was observed for the related diyne complex $Co_2(\mu\text{-}\eta^2\text{-}PhC_2C{\equiv}CPh)(CO)_4$(dppm), although the reduction wave was irreversible in CH_2Cl_2.[16b]

For each of the heterometallic complexes **4** and **5** a single, reversible, one-electron reduction wave was observed (−1.29 V **4**, −1.36 V **5**) as well as two quasi-reversible oxidation processes $E_{Ox1}°$ (+0.96 V **4**, +0.86 V **5**) and $E_{Ox2}°$ (+1.16 V **4**, +1.14 V **5**) (Table 4, Figure 7). The close spacing of the oxidation waves hindered meaningful determination of the peak current ratio for E_{Ox2}. However, in both cases, chemical reactions followed E_{Ox2}, and minor product reduction processes were observed at $E_{pc(A)}$ 0.31 V (**4**) and at $E_{pc(B)}$ 0.52 V and $E_{pc(C)}$ 0.12 V (**5**). These reduction waves A, and B and C are not observed when the reverse sweep in the cyclic voltammograms were initiated prior to the generation of $[\mathbf{4}]^{2+}$ or $[\mathbf{5}]^{2+}$ at potentials near E_{Ox2}. The identification of these electrogenerated chemical species must await the results of a more detailed spectroelectrochemical study.

It is reasonable to attribute the reduction processes in **4** and **5** to the $[Co_2C_2]^{0/-}$ couple, although these reductions occur at a more negative potential than the analogous process in the parent complexes **2** and **3** (Table 4). On this basis **4** and **5** are predicted to have a Co_2C_2-centered LUMO, which is somewhat raised in energy when compared with **2** and **3**.

More information about the nature of the electronic interaction between the metal fragments is contained in the oxidative sweep, as model compounds for each of the isolated parts of the molecule (**2** or **3** and **6**) display an oxidation wave. Both oxidation processes in **4** and **5** occur at much less positive potentials than the $[Co_2C_2]^{0/+}$ couple in the precursors **2** and **3**, respectively, and also at a less positive potential than the $Ru^{II/III}$ couple of the model complex $Ru(C{\equiv}CPh)(PPh_3)_2Cp$ ($E°$ +1.10 V) (Table 4).

Consider a hypothetical case in which the redox-active centers are completely independent (i.e., there are no interactions between the $Ru(PPh_3)_2Cp$ and Co_2C_2 moieties). In such a case, the $E°$ values for the $Ru^{II/III}$ and $[Co_2C_2]^{0/+}$ couples in **4** or **5** would be essentially identical to the $E°$ values observed for the isolated components, with small differences due to the modified solvent interactions about each redox-active core resulting from the new molecular shape. It is apparent from the data collected in Table 4 that this is not the case, and the organometallic moieties in **4** and **5** must therefore interact in some fashion.

If the Ru and Co_2C_2 oxidation centers are considered to interact via a simple through-space (i.e., Coulombic) mechanism, the first oxidation process, which yields a positively charged pendant group, should result in a less thermodynamically favorable second oxidation when compared to the isolated parent species. Again, this simple model fails to satisfy the experimental data.

We find that a more subtle, through-bond mechanism of interaction is required to explain the presence of two one-electron oxidation processes in **4** and **5**, both of which are thermodynamically more favorable than in the isolated model complexes **2** or **3** and **6**. To resolve this issue, and address the broader issues about the nature of the electronic interactions occurring between

(46) (a) Beddoes, R. L.; Bitcon, C.; Ricalton, A.; Whiteley, M. W. *J. Organomet. Chem.* **1989**, *367*, C21. (b) Bitcon, C.; Whiteley, M. W. *J. Organomet. Chem.* **1987**, *336*, 385.

Table 5. Selected Bond Lengths (Å) Obtained from Optimized Structure Models, and Charges on Various Fragments[g]

	Ru−C	C≡C[a]	C−C[b]	Co−Co	Σq_D	Σq_B	Σq_A
A			1.35 (1.34)	2.47 (2.46)			
B			1.37 (1.36)	2.47 (2.48)			
C	1.99 (1.98)	1.25 (1.23)	1.37 (1.37)	2.47 (2.48)	+0.50	−0.37	−0.13
D	1.99 (1.99)	1.25 (1.22)	1.38 (1.37)	(2.47)	+0.52	−0.34	−0.18
E	2.01	1.24			+0.43	−0.54	+0.21
F	2.02 (2.01)[c]	1.24 (1.21)[c]			+0.45	−0.38	−0.07
G	2.00 (1.99)[d]	1.25 (1.23)[d]			+0.49	−0.34	−0.15
H		1.22 (1.205[e], 1.218[f])					

[a] C≡C of acetylene directly attached to Ru. [b] C−C of the Co_2C_2 cluster. [c] From ref 42. [d] From ref 48. [e] Callomon, J. H.; Stoicheff, B. P. *Can. J. Phys.* **1957**, *35*, 373. [f] Tanimoto, M.; Kuchitsu, K.; Morino, Y. *Bull. Chem. Soc. Jpn.* **1971**, *44*, 386. [g] Average values of the experimental parameters are included in parentheses where appropriate. See text for chemical formula of model species and definition of symbolism.

the organometallic fragments in more detail, a thorough theoretical analysis was undertaken.

Theoretical Studies. To facilitate theoretical analysis, several simplified structural models have been adopted. Thus, calculations have been performed on $Co_2(\mu\text{-}HC_2H)(CO)_6$ (**A**) and $Co_2(\mu\text{-}HC_2H)(CO)_4(H_2PCH_2PH_2)$ (**B**), which serve as structural models for **2** and **3**, and $Co_2\{\mu\text{-}H_3SiC_2C{\equiv}CC{\equiv}C[Ru(PH_3)_2Cp]\}(CO)_4(H_2PCH_2PH_2)$ (**C**) and $Co_2\{\mu\text{-}H_3SiC{\equiv}CC_2C{\equiv}C[Ru(PH_3)_2Cp]\}(CO)_4(H_2PCH_2PH_2)$ (**D**), which model **4** and **5**, respectively. In addition, $Ru(C{\equiv}CR)(PH_3)_2Cp$ (R = H (**E**); Ph (**F**); $C_6H_4NO_2$-*p* (**G**)) and HC≡CC≡CH (buta-1,3-diyne) (**H**) were also modeled as reference compounds. The model compounds were subjected to geometry optimization, as detailed in the Experimental Section. Quantitative agreement between the observed and calculated data is not expected due to the nature of the theoretical and structural approximations. However, the model compounds do provide an effective method for probing the electronic structures and spectroscopic and electrochemical properties of the experimental compounds and provide an indication of the various structure−property relationships.

Several relevant structural parameters obtained from the optimized structures of **A**−**H** are compared with the experimental data in Table 5. The computed Ru−C distance in **C** and **D** is found to be relatively short (1.99 Å), while the corresponding C≡C separation is somewhat long (1.25 Å). However, the calculations reproduce the increase in C−C length in the cluster backbone upon substitution of two CO ligands in **A** (1.35 Å) for $H_2PCH_2PH_2$ in **B** (1.37 Å), **C** (1.37 Å), and **D** (1.38 Å) found in the experimental analogues. The Co−Co bond length in all of the model compounds was found to be unaffected by phosphine substitution (2.47 Å). It is notable that the absolute values of these parameters, as well as the trends across the series, are in excellent agreement with the crystallographically determined parameters. This observation provides a measure of confidence in the accuracy of the computations and, hence, the conclusions that are drawn from them.

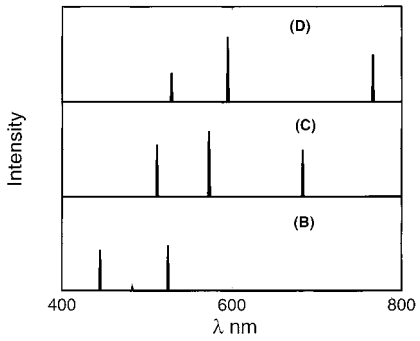

Figure 8. Calculated UV/vis spectra of model compounds **B**, **C**, and **D**. Intensities are in arbitrary units.

The calculated UV/vis absorption spectra in the region of 400−800 nm are presented in Figure 8. The visible region of the spectrum for **B**, **C**, and **D** each contains three distinct absorptions. For **B** these absorptions (445, 485, and 525 nm) all correspond to excitations from the Co_2C_2 cluster HOMO to an unoccupied Co_2C_2-based orbital. In **C**, the transitions that give rise to the optical bands arise from an orbital that has the same gross shape as the corresponding orbital in **B**, but also contains a small, yet significant, contribution from the Ru−C≡CC≡C moiety. This secondary mixing leads to a destabilization of this essentially Co_2C_2-centered orbital in **C** with respect to that in **B**. Consequently, the UV−vis spectrum of **C** also contains three similar transitions (512, 575, and 683 nm) which are strongly red shifted relative to those observed in **B**. Furthermore, the intensity ratio of the peaks has also changed due to a remixing of the orbitals. However, one fact does remain consistent: the transitions remain localized on orbitals centered on the Co_2C_2 cluster core and have no contribution either in the occupied or unoccupied states from Ru. These same three transitions also occur in the spectrum of **D** (529, 595, and 766 nm) and are even more red shifted then those of **C**, as a result of a greater contribution from the acetylenic moiety. The trend in these spectral shifts is strongly correlated with those observed in the experimental species. More quantitative agreement between the experimental data and the computed spectra should not be expected due to the use of the approximated structural models in the gas phase. However, the qualitative agreement between the experimental and computational results strongly suggests that the observed change in color is due primarily to a reorganization of the energy levels of the Co_2C_2 cluster core rather than a Ru cluster charge-transfer process.

A schematic MO diagram of the frontier orbitals of **A**−**E** is presented in Figure 9. The frontier orbitals of the model complex **A** have been well established by Hoffman, Hoffmann, and Fisel[47] and others. These orbitals are reproduced by the current DFT treatment, although there is a small discrepancy in the ordering of the occupied orbitals below the HOMO. These orbitals retain their overall shape and order in compound **B** but

(47) (a) Hoffman, D. F.; Hoffmann, R.; Fisel, C. R. *J. Am. Chem. Soc.* **1982**, *82*, 3858. For further discussion see for example: (b) Thron, D. L.; Hoffmann, R. *Inorg. Chem.* **1978**, *17*, 126. (c) DeKock, R. L.; Lubben, T. V.; Hwang, J.; Fehlner, T. P. *Inorg. Chem.* **1981**, *20*, 1627. (d) Baert, F.; Guelzim, A.; Poblet, J. M.; Wiest, R.; Demuynck, J.; Bunard, M. *Inorg. Chem.* **1986**, *25*, 1830. (e) Pepermans, H.; Hoogzand, C.; Geerlings, P. *J. Organomet. Chem.* **1986**, *306*, 395. (f) Halet, J.-F.; Saillard, J.-Y. *J. Organomet. Chem.* **1987**, *327*, 365. (g) Yuan, P.; Don, M.-J.; Richmond, M. G.; Schwartz, M. *Inorg. Chem.* **1992**, *31*, 3491.

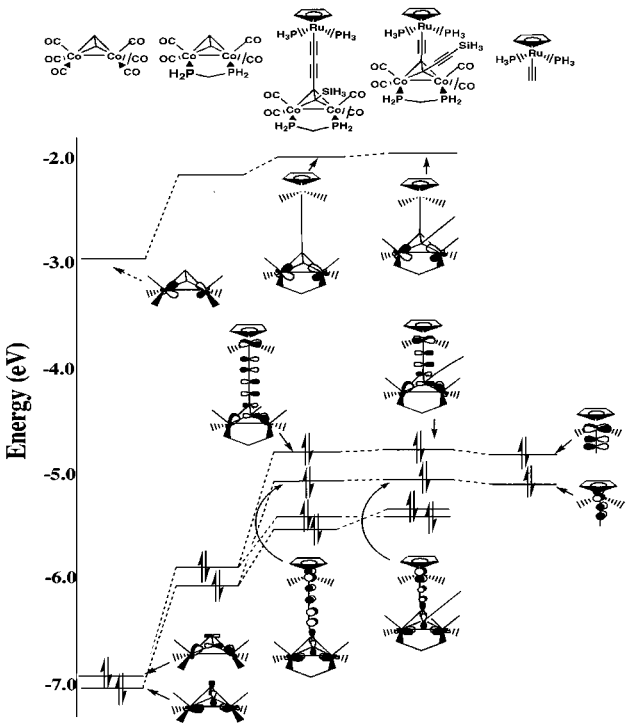

Figure 9. Schematic MO diagram of frontier orbitals of compounds **A**−**E**.

are increased in energy about 1 eV, which is consistent with the presence of the electron-donating $H_2PCH_2PH_2$ ligand. This shift also correlates well with the lower oxidation and higher reduction potentials observed in the electrochemical measurements on related systems (vide supra).

The frontier orbitals of **E** are also well established,[48] and these earlier results are essentially reproduced by the DFT scheme employed in this work. The HOMOs and SHOMOs of **C** and **D** are, approximately, the same as found for **E** (Figure 9). However, two important differences must be highlighted. First, the energy of the HOMO increases in the order **E** < **C** < **D**, which, assuming that electrochemical oxidation involves removal of electrons from the HOMO, is in good agreement with the electrochemical measurements (Table 4 and above discussion). Second, these HOMOs include significant contributions from not only the $Ru(PH_3)_2Cp$ fragment and the acetylenic moiety but also the Co_2C_2 cluster core. As a result, the HOMO is actually delocalized across the entire molecule. However, it is important to note that in both **C** and **D** the HOMO is not bonding in nature, but consists primarily of a Ru−C(acetylene) antibonding interaction and a similar antibonding interaction between the acetylene backbone and the Co_2C_2 cluster. This orbital picture suggests that there is very little direct "communication" between the Ru center and the Co_2C_2 cluster core in terms of a delocalized bonding model (Figure 10a). Instead, a description involving a more inductive interaction between the two fragments passed on via a filled orbital−filled orbital repulsive interaction along the acetylenic bridge (Figure 10b) appears to be more justified. This also correlates well with our interpretation of the trends

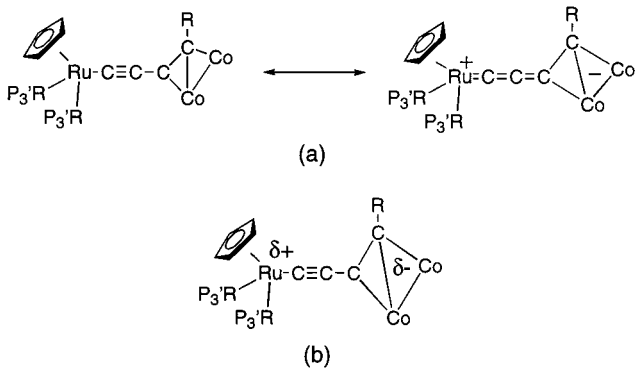

Figure 10. Electronic interactions between the $Ru(PPh_3)_2$-Cp fragment and $Co_2C_2(CO)_4$(dppm) cluster core represented in terms of (a) a bonding electron delocalized model and (b) an inductive model.

of the UV/vis absorption as obtained from ZINDO calculations (vide supra) and also matches the observation of characteristic ν(C≡C) bands in the IR spectra of **4** and **5** (Table 3).

To provide further support for this conclusion, a description of the electron density about the acetylenic C≡C moieties that link the organometallic fragments was undertaken using the electron localization function (ELF), which is defined as[49]

$$\eta(r) = \frac{1}{\left(1 + \left(\frac{\sum_i |\nabla\Psi_i|^2 - \frac{1}{4}\frac{(\nabla\rho)^2}{\rho}}{\frac{3}{5}(3\pi^2)^{5/3}\rho^{5/3}}\right)^2\right)}$$

The ELF method puts electron localization onto a quantitative footing while managing to avoid some of the inherent difficulties that may arise in traditional orbital-based analysis. The ELF function, $\eta(r)$, is large in regions where two electrons with antiparallel spin are paired in space, and hence its maxima can be associated with attractor basins due to electron pairing. The ELF is normalized between zero and unity, with the value for a uniform electron gas being 1/2. This normalization scale allows for the direct comparison of electron localization between similar atoms in different chemical systems and thus places the concept of the localization of electrons on a semiquantitative footing. Consequently, the ELF has met with great success when used as a tool to locate and interpret chemical bonding in a variety of different systems.[50] To understand the information contained in this function in greater detail, one may consider, for example, a core state in an atom as a typical *localized* electronic state. The local kinetic energy density $\sum_i|\nabla\phi|^2$ will be very high, but so will the gradient of the electronic density $\nabla\rho(r)$. In such a case

(48) McGrady, J. E.; Lovell, T.; Stranger, R.; Humphrey, M. G. *Organometallics* **1997**, *16*, 4004.

(49) Becke, A. D.; Edgecombe, K. E. *J. Chem. Phys.* **1990**, *92*, 5397.

(50) (a) Silvi, B.; Savin, A. *Nature (London)* **1994**, *371*, 683. (b) Savin, A.; Jepsen, O.; Flad, J.; Andersen, O. K.; Preu, H.; von Schnering, H. G. *Angew. Chem., Int. Ed. Engl.* **1992**, *31*, 187. (c) Savin, A.; Nesper, R.; Wengert, S.; Fõssler, T. F. *Angew. Chem., Int. Ed. Engl.* **1997**, *36*, 1808. (d) Savin, A.; Becke, A. D.; Flad, J.; Nesper, R.; Preuss, H.; von Schnering, H. G. *Angew. Chem., Int. Ed. Engl.* **1991**, *30*, 409. (e) Marx, D.; Savin, A. *Angew. Chem., Int. Ed. Engl.* **1997**, *36*, 2077.

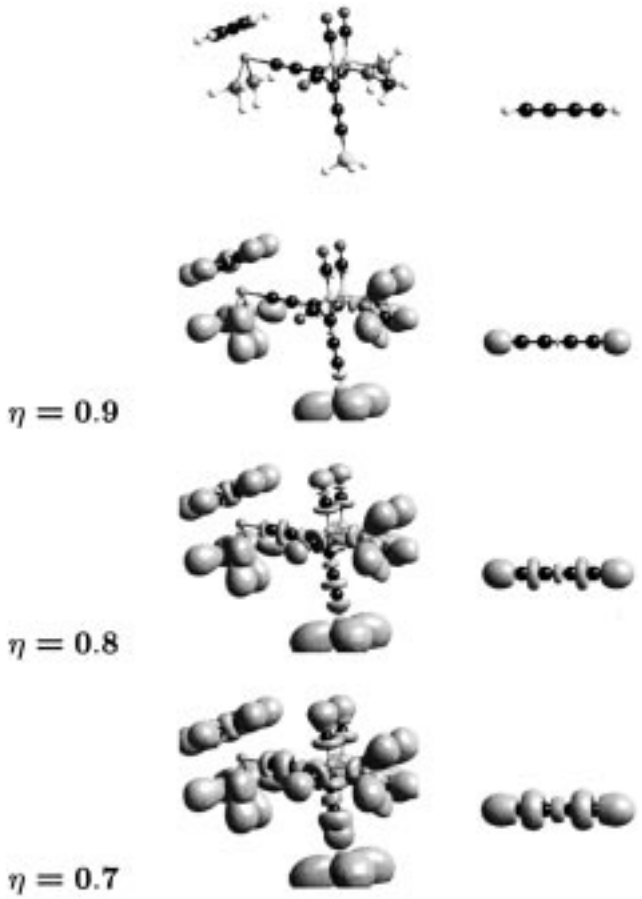

Figure 11. Electron localization function plotted as isosurfaces $\eta = 0.9$, 0.8, and 0.7 for model compounds **D** and **H**.

these two terms effectively cancel each other and $\eta(r) \approx 1.0$. On the other hand, a valence electron in a conduction band of a metal, which may be regarded as a prototypical *delocalized* state, will have a larger kinetic energy density relative to the gradient of $\rho(r)$ and consequently a lower value of $\eta(r)$. In essence, the ELF will identify features such as lone electron pairs and multiple bonds between elements and is therefore an ideal instrument with which to probe the nature of the bonding along the carbon bridge in **C** and **D**.

The ELF for the model compounds **D** and **H** is plotted as a series of isosurfaces, $\eta = 0.9$, 0.8, and 0.7, in Figure 11. The most localized bonding regions in both compounds occur for spatial regions that correspond to the C−H, P−H, and Si−H σ-bonds ($\eta^{max} \approx 1.0$), as one would intuitively expect. For **D**, the next highest ELF maxima ($\eta^{max} \approx 0.93-0.96$) correspond to the P−C and Si−C σ-bonds and the lone pairs on the P atoms, which are directed toward the Ru and Co centers. At lower values of η^{max} ($\eta^{max} \approx 0.90-0.92$) the C−C bonds in the Cp ring and the Co−CO bonds in **D** and all of the remaining C−C single bonds in both **D** and **H** are identified. It is important to note that the central C−C bond in **H** has exactly the same value of $\eta^{max} = 0.91$ as both the corresponding bond in **D** and the C−C bond in the Co_2C_2 cluster. As we move to still lower values of ELF, the regions of space corresponding to oxygen lone pairs and the Ru−C bond appear ($\eta^{max} = 0.89$). The next and most striking feature of our ELF analysis is the emergence of the ring-shaped C≡C attractor in both **D** and **H** at exactly the same value of $\eta^{max} = 0.87$. Thus, while the C≡C bond length is greater in **D** than in **H** (Table 5), the localization properties of the bonds are identical. The last two sets of attractors to appear in **D** are associated with the C−O ligands ($\eta^{max} = 0.83$) and the four Co−C bonds of the Co_2C_2 cluster core ($\eta^{max} = 0.82$) The cluster-based attractor basins collapse into a single region of localization at $\eta = 0.8$. For values of the ELF lower than 0.8 all of the distinct regions of electron pairing indicated above begin to collapse into each other, forming larger domains stretching over the various functional groups. It may be noted that the acetylene-based bridge in **D** behaves in exactly the same manner as **H**, with the C≡C and C−C bonding regions touching in both cases at exactly $\eta = 0.71$, and reinforces the claim that the electron localization along the acetylenic chain is similar in **D** and **H**.

It is also important to consider the shape of the various attractor basins.[50a] We note that the Co−CO bonds in **D** have the shape of a ring, which is distorted around the carbon nucleus due to the CO π^* component of the metal−carbonyl back-bond.[50a] Similarly, the C p-orbital component of the C≡C bonds in **H** results in a ring-shaped attractor basin in this region of space. In the case of regions of electron density void of π (or p) character, such as the C−C single bond of **H**, the attractor basins are not ring shaped, but are rather more shaped like a solid disk (Figure 11). The bonding attractors located between the phosphine ligands and the metal centers are also disk-shaped, which is a manifestation of the good σ-donating, poor π-accepting character of the phosphine.

The shapes of the bonding attractors associated with the Ru−C≡C−Co_2C_2 portion of **D** therefore reveal a great deal of information about the bonding within the molecule and nature of the electronic interaction between the organometallic fragments. The attractors associated with the Ru−C and C−Co_2C_2 bonds, and the C−C bond of the metallocarbon cluster, are all disk-shaped, indicating that these bonds have negligible π-character. In contrast, the bonding attractor arising from the C≡C moiety has the same ring shape as found for the analogous feature in **H**.

On the basis of the identical η^{max} behavior and similar shapes of the attractor basins associated with the Ru−*C*≡*C*−Co_2C_2 alkynyl portion of **D** and the acetylenic fragments in **H**, we must conclude that the electron density in each C≡C moiety is localized in an identical manner. Taken all in all, this pattern of electron localization is entirely consistent with the interpretation presented in Figure 10b and, moreover, rules out an interpretation of the interaction based on the cumulenic structure represented in Figure 10a. This assertion is further supported by our natural bond orbital population analysis (vide infra) that indicates no appreciable Ru−C π-bonding or back-bonding.

Compounds **C**−**G** may be thought of as containing three distinct portions: a donor fragment $Ru(PH_3)_2Cp$ (*D*), an acetylene bridge (*B*), and an acceptor fragment (*A*) (*A* = C≡C($Co_2C_2(CO)_4(H_2PCH_2PH_2)SiH_3$, **C**; Co_2C_2-$(CO)_4(H_2PCH_2PH_2)$C≡CSiH_3, **D**; H, **E**; Ph, **F**; $C_6H_4NO_2$-*p*, **G**). For **C**−**G**, the net charge on each fragment $\sum q_D$, $\sum q_B$, and $\sum q_A$ has been derived by summation of the atomic charges, which were in turn obtained from a

natural atomic orbital population analysis (Table 5). With the exception of **E**, the net charge on the bridge *B* remains relatively constant. The compounds with larger positive charges on *D* also feature correspondingly large negative charge on *A*, indicating that the role of the bridge is to aid in the stabilization of a charge-transfer state. In the case of **E**, the poor electron-accepting properties of the terminal hydrogen results instead in an increase in negative charge on the bridge. A comparison of $\sum q_D$ and the bond lengths reported in Table 5 indicates that the larger the positive charge of *D*, the shorter the Ru−C bond and suggests that the observed structural trends are due to an essentially electrostatic effect.

Finally we note that the computed charges indicate that compound **D** will have a more effective transfer of charge than found in **C**, and thus its properties will be more significantly affected, as seen in their experimental analogues. This model of a stabilized charge-transfer state is in line with the suggestion previously made for **G**,[48] and the magnitude of the effect is comparable in **C**, **D**, and **G**.

Conclusion

The complexes **4** and **5** are affected to a significant extent by the donor/acceptor character of the $Ru(PPh_3)_2Cp$ and $Co_2C_2(CO)_4(Ph_2PCH_2PPh_2)$ fragments when linked by an acetylenic bridging ligand. The degree of charge separation is on a par with that previously observed between the Ru moiety and the classic organic acceptor $C_6H_4NO_2$-*p* and is best described using a model based on inductive effects.

The orbital description obtained from DFT and ELF studies suggests that the degree of interaction may be modified in a rational manner and that increasing the electron density at the Ru center (by substitution of PPh_3 for PMe_3) or decreasing the effective electron density at the Co_2C_2 core (by replacing the dppm ligand with two CO ligands) will lead to even more pronounced interactions. Studies along these lines are currently being pursued.

Experimental Section

General Conditions. All reactions were carried out under dry high-purity nitrogen using standard Schlenk techniques. Solvents were dried, distilled, and degassed prior to use. Preparative TLC was performed on 20 × 20 cm glass plates coated with silica gel (CAMAG DSF-5, 0.5 mm thick). Literature methods were used to prepare $Me_3SiC{\equiv}CC{\equiv}CC{\equiv}CSiMe_3$,[51] $Co_2(CO)_6(dppm)$,[52] and $RuCl(PPh_3)_2Cp$.[53] Other reagents were purchased and used as received.

Instrumental Measurements. Infrared spectra were recorded using calcium fluoride cells of 0.5 mm path length. UV−vis spectra were recorded from thf solutions in a 1 cm path length cuvette. NMR spectra were recorded at (^{1}H) 400.13 MHz and (^{13}C) 100.61 MHz in $CDCl_3$ and referenced against the solvent resonances. FAB-MS were obtained using Xe as the exciting gas, FAB gun voltage 6 kV, accelerating potential 3 kV, and *m*-nitrobenzyl alcohol matrix. Cyclic votammetry experiments were carried out in thf containing 0.5 M $[^nBu_4N][BF_4]$. Solutions (1×10^{-3} M) were purged with nitrogen and measured versus a Ag/Ag^+ reference electrode at −50 °C, such that the ferrocene/ferrocenium redox couple was located at 0.99 V. Microanalyses were performed at the NRC's Institute for Biological Sciences, 100 Sussex Dr., Ottawa, Ontario, K1A 0R6, Canada.

Reaction of $Me_3SiC{\equiv}CC{\equiv}CC{\equiv}CSiMe_3$ with $Co_2(CO)_6$-(dppm). A solution of $Co_2(CO)_6(dppm)$ (660 mg, 0.98 mmol) and $Me_3SiC{\equiv}CC{\equiv}CC{\equiv}CSiMe_3$ (200 mg, 0.91 mmol) in benzene (70 mL) was heated at reflux for 2 h. After this time TLC analysis indicated the complete consumption of starting material. The reaction mixture was adsorbed onto a small amount of silica gel and the reaction mixture purified by column chromatography on silica gel. A hexane/CH_2Cl_2 gradiant (0−30% CH_2Cl_2) resolved two bands. The first red-brown band was crystallized (CH_2Cl_2/MeOH slow evaporation) to give dark red, needlelike crystals of $Co_2(\mu\text{-}\eta^2,\eta^2\text{-}Me_3SiC_2C{\equiv}CC{\equiv}CSiMe_3)(CO)_4(dppm)$ (**2**) (125 mg, 17%). The second red band gave red, block-shaped crystals of $Co_2(\mu\text{-}\eta^2,\eta^2{:}\mu\text{-}\eta^2,\eta^2\text{-}Me_3SiC{\equiv}CC_2C{\equiv}CSiMe_3)(CO)_4(dppm)$ (**3**) (348 mg, 46%) (CH_2Cl_2/MeOH slow evaporation). **2** found: C, 60.34; H, 5.19. $Co_2Si_2P_2O_4C_{41}H_{40}$ requires: C, 59.13; H, 4.84. IR (cyclohexane): ν(C≡C) 2160w,-br; ν(CO) 2030vs, 2009vs, 2004sh, 1982vs, 1962w cm^{-1}. ^{1}H NMR ($CDCl_3$): δ 0.30, 0.37 (2 × s, 2 × 9H, 2 × $SiMe_3$); 3.11 (dt, J_{HP} = 12 Hz, J_{HH} = 10 Hz, CH_2P_2) 3.92 (dt, J_{HP} = 12 Hz, J_{HH} = 10 Hz, CH_2P_2); 7.15−7.42 (m, 20H, Ph). ^{13}C NMR ($CDCl_3$): δ 0.87, 1.57 (2 × s, 2 × $SiMe_3$); 37.99 (t, J_{CP} = 20 Hz, CH_2P_2); 75.41 [t, J_{CP} = 8 Hz, C(5/6)]; 82.39 [t, J_{CP} = 4 Hz, C(5/6)]; 81.48, 91.34, 91.55, 92.89 (4 × s, 4 × C≡C); 127.97−137.98 (m, Ph); 201.96, 207.88 (2 × br, CO). FAB-MS (*m*/*z*): 832 $[M]^+$, 804−720 $[M - nCO]^+$ (n = 1−4). **3** found: C, 58.55; H, 4.86. $Co_2Si_2P_2O_4C_{41}H_{40}$ requires: C, 59.13; H, 4.84. IR (cyclohexane): ν(C≡C) 2118w, 2105w; ν(CO) 2037s, 2019vs, 1994vs, 1972w cm^{-1}. ^{1}H NMR ($CDCl_3$): δ 0.29 (s, 9H, $SiMe_3$); 3.44 (t, J_{HP} = 5 Hz, 1H, CH_2P_2); 7.22−7.36 (m, 20H, Ph). ^{13}C NMR ($CDCl_3$): δ 0.44 (s, $SiMe_3$); 34.31 (t, J_{CP} = 21 Hz); 70.37 [br, C(5/6)], 103.27, 107.85 (2 × s, 2 × C≡C); 127.54−136.13 (m, Ph); 203.83 (br, CO). FAB-MS (*m*/*z*): 832 $[M]^+$; 804−720 $[M - nCO]^+$ (n = 1−4).

$Co_2\{\mu\text{-}Me_3SiC_2C{\equiv}CC{\equiv}C[Ru(PPh_3)_2Cp]\}(CO)_4(dppm)$ (4). A solution of $RuCl(PPh_3)_2Cp$ (35 mg, 0.048 mmol) and **2** (48 mg, 0.048 mmol) in thf (7 mL)/MeOH (7 mL) was treated with KF (ca. 5 mg) and heated at reflux for 1 h. The solvent was removed and the residue purified by preparative TLC (10% acetone in hexane) to give a single brown band, which was crystallized (acetone/hexane) to afford $Co_2\{\mu\text{-}Me_3SiC_2C{\equiv}CC{\equiv}C[Ru(PPh_3)_2Cp]\}(CO)_4(dppm)$ (**4**) (55 mg, 79%) as dark greenish-brown needles. Found: C, 65.65; H 4.53. $RuCo_2SiP_4O_4C_{79}H_{64}$ requires: C, 65.46; H, 4.45. IR (cyclohexane): ν(C≡C) 2124w; ν(CO) 2018m, 1998vs, 1970s, 1952w cm^{-1}. ^{1}H NMR ($CDCl_3$): δ 0.78 (s, 9H, $SiMe_3$); 3.43 (br, 2H, CH_2P_2); 4.55 (s, 5H, Cp); 6.87−7.80 (m, 50H, Ph). ^{13}C NMR ($CDCl_3$): δ 1.21 (s, $SiMe_3$); 36.82 (t, J_{CP} = 20 Hz, CH_2P_2); 64.69 (br, C(4)); 84.68 (t, J_{CP} = 9 Hz, C(5/6)); 86.41 (s, Cp); 89.72 (t, J_{CP} = 5 Hz, C(5/6)); 89.82 (s, C(3)); 90.09 (t, J_{CP} =16 Hz, C(1)); 100.08 (s, C(2)); 127.97−138.99 (m, Ph); 203.19, 208.32 (2 × br, 2 × CO). FAB-MS (*m*/*z*): 1450, $[M + H]^+$; 1422−1338, $[M - nCO]^+$ (n = 1−4); 1188, 1104, 1076, $[M - PPh_3 - nCO]^+$ (n = 0,3,4); 926, 842, 814, $[M - 2PPh_3 - nCO]^+$ (n = 0, 3, 4).

$Co_2\{\mu\text{-}Me_3SiC{\equiv}CC_2C{\equiv}C[Ru(PPh_3)_2Cp]\}(CO)_4(dppm)$ (5). A solution of **3** (103 mg, 0.103 mmol) in thf (5 mL)/MeOH (10 mL) was treated with $RuCl(PPh_3)_2Cp$ (75 mg, 0.103 mmol) and KF (ca. 10 mg). The mixture was heated at reflux for 3 h, during which time the solution color changed from red to dark green. The solvent was removed and the residue purified by preparative TLC (10% acetone in hexane). The major dark green band yielded $Co_2\{\mu\text{-}Me_3SiC{\equiv}CC_2C{\equiv}C[Ru(PPh_3)_2Cp]\}(CO)_4(dppm)$ (**5**) (110 mg, 74%) as dark green blocks following crystallization (acetone/hexane, slow diffusion). Found: C, 65.03; H, 4.95. $RuCo_2SiP_4O_4C_{79}H_{64}$ requires: C, 65.46; H 4.45. IR (cyclohexane): ν(C≡C) 2104w; ν(CO) 2036s, 2015m, 2000vs, 1975s, 1954vw cm^{-1}. ^{1}H NMR ($CDCl_3$): δ 0.47 (s, 9H, $SiMe_3$);

(51) Rubin, Y.; Lin, S. S.; Knobler, C. B.; Anthony, J.; Doldi, A. M.; Diederich, F. *J. Am. Chem. Soc.* **1991**, *113*, 6943.
(52) Chia, L. S.; Cullen, W. R. *Inorg. Chem.* **1975**, *14*, 482.
(53) Bruce, M. I.; Hameister, C.; Swincer, A. G.; Wallis, R. C. *Inorg. Synth.* **1990**, *28*, 270.

3.10 (br, 1H, CH_2P_2); 3.79 (dt, $J_{HP} = J_{HH} = 11$ Hz); 4.55 (s, 5H, Cp); 6.87−7.91 (m, Ph). ^{13}C NMR ($CDCl_3$): δ 1.04 (s, $SiMe_3$); 34.52 (t, $J_{CP} = 21$ Hz, CH_2P_2); 95.78, 99.75 (2 × s, C(5/6)); 111.08 (t, $J_{CP} = 4$ Hz, C(1)); 114.78 (s, C(2)); 127.78−139.67 (m, Ph); 203.33, 208.64 (2 × br, 2 × CO). FAB-MS (*m*/*z*): 1450, $[M + H]^+$; 1421−1337, $[M - nCO]^+$ ($n = 1-3$); 1103 $[M - 3CO - PPh_3]^+$, 1075 $[M - 4CO - PPh_3]^+$.

Crystallography. Data were collected on a Siemens SMART CCD diffractometer. Unique diffractometer data sets (monochromatic Mo Kα radiation, $\lambda = 0.7107_3$ Å; ω scan mode; $T = 173$ K) were measured within the specified $2\theta_{max}$ limit yielding N independent reflections, N_o of these with $I > 2.0\sigma(I)$ being considered observed and used in the block/full-matrix least-squares refinement after an empirical absorption correction utilizing the SADABS routine associated with the Siemens diffractometer. Anisotropic thermal parameters were refined for the non-hydrogen atoms. In the final cycles of refinement hydrogen atoms were placed in calculated positions and constrained with a riding model. The minimized function was $\sum w(F_o^2 - F_c^2)^2$. Computations were performed using the SHELXTL suite of programs.[54] For **2**, two independent molecules were contained within the unit cell. These differed only by the relative orientation of a phenyl ring, and molecular parameters were equivalent within error. The Si(1) trimethylsilyl fragment was disordered over two sites, which were successfully modeled at 72:28 occupancy following trial refinement. The analogous Si(21)Me_3 fragment in the second molecule was treated similarly. Residual electron density in **4** was successfully modeled as a molecule of a hexane solvate, with 50% occupancy. The unit cell of **5** contained two fully occupied molecules of acetone, which were refined without difficulty. In the absence of high-angle data, the 2θ range for **2** and **4** were constrained to a maximum value of 45° and 50°, respectively.

Computational Details. Geometry optimization on the model compounds was performed within the Kohn−Sham description of density functional theory.[55] In particular, the B3LYP hybrid Hartree−Fock DFT method[56] was employed as implemented within the Gaussian 94 software package[57] with a LanL2DZ basis set.[58] Criteria for optimization were chosen as the defaults of this package. Population analysis was performed within the formalism of natural orbitals.[59] Electronic absorption spectra were simulated by performing ZINDO calculations,[60] as implemented within the Hyperchem package,[61] on the DFT optimized structures. The orbital manifold for the UV/vis calculations was increased systematically until the spectra were converged within the 400−800 nm range. Topological analysis on the electron density was performed in terms of the electron localization function (ELF) of Becke and Edgecombe,[49] as implemented in the Vienna ab initio simulation package (VASP),[62] again on the static structures obtained from the geometry optimization. For these later calculations, the local density approximation was employed, with the core electrons replaced via Vanderbelt ultrasoft pseudopotentials.[63] The molecule was placed within a 16 Å cubic box subject to periodic boundary conditions, and the valence electrons expanded within a basis set of plane waves with an energy cutoff of 30 Ry.

Acknowledgment. We gratefully acknowledge financial support from the National Research Council Canada (NRC) and the Natural Sciences and Engineering Research Council (NSERC). P.J.L. holds an NSERC-NRC Canadian Government Laboratories Visiting Fellowship.

Supporting Information Available: Tables of crystal data collection and refinement details, positional and thermal parameters, and bond distances and angles for **2**, **3**, **4**, and **5**, and Cartesian coordinates of all optimized geometries. This material is available free of charge via the Internet at http://pubs.acs.org. Structure factors are available from the authors upon request.

OM990290W

(54) (a) Sheldrick, G. M. *Acta Crystallogr.* **1990**, *A46*, 467. (b) Sheldrick, G. M. *Acta Crystallogr.* **1993**, *A49* (Suppl.), C53.

(55) (a) Parr, R. G.; Yang, W. *Density-Functional Theory of Atoms and Molecules*; Oxford University Press: Oxford, 1989. (b) Jones, R. O.; Gunnarsson, O. *Rev. Mod. Phys.* **1989**, *61*, 689.

(56) Becke, A. D. *J. Chem. Phys.* **1993**, *98*, 5648.

(57) Frisch, M. J.; Trucks, G. W.; Schlegel, H. B.; Gill, P. M. W.; Johnson, B. G.; Robb, M. A.; Cheeseman, J. R.; Keith, T.; Petersson, G. A.; Montgomery, J. A.; Raghavachari, K.; Al-Laham, M. A.; Zakrzewski, V. G.; Ortiz, J. V.; Foresman, J. B.; Peng, C. Y.; Ayala, P. Y.; Chen, W.; Wong, M. W.; Andres, J. L.; Replogle, E. S.; Gomperts, R.; Martin, R. L.; Fox, D. J.; Binkley, J. S.; Defrees, D. J.; Baker, J.; Stewart, J. P.; Head-Gordon, M.; Gonzalez, C.; Pople, J. A. *Gaussian 94, Revision B.2*; Gaussian, Inc.: Pittsburgh, PA, 1995.

(58) Hay, P. J.; Wadt, W. R. *J. Chem. Phys.* **1985**, *82*, 270, 299.

(59) Reed, A. E.; Curtiss, L. A.; Weinhold, F. *Chem. Rev.* **1988**, *88*, 899.

(60) Anderson, W. P.; Edwards, W. D.; Zerner, M. C. *Inorg. Chem.* **1985**, *25*, 2728.

(61) *Hyperchem*, Release 4.5 for Silicon Graphics workstations; Hypercube Inc.: Aug 1995.

(62) (a) Kresse, G.; Hafner, J. *Phys. Rev. B* **1993**, *47*, 55; **1994**, *49*, 14251. (b) Kresse, G.; Furthmuller, J. *Comput. Mater. Sci.* **1995**, *6*, 15. Kresse, G.; Furthmuller, J. *Phys. Rev. B* **1996**, *54*, 11169.

(63) Vanderbelt, D. *Phys. Rev. B* **1990**, *41*, 7892. The pseudopotentials used were those taken from the database provided with the VASP program.